SUPPLEMENTARY ONLINE MATERIAL

Fluorescence imaging of cellular metabolites with RNA

Jeremy S. Paige, Thinh Nguyen Duc, Wenjiao Song, and Samie R. Jaffrey

Contents:

SUPPLEMENTARY DISCUSSION

Design of transducer modules for Spinach-based sensors. The metabolite-binding aptamers used in this study have been previously characterized (*1-4*). Screening for optimal transducer modules was based on their ability to induce fluorescence in a metabolite-dependent manner. The optimal sensors were chosen based on their low fluorescence in the absence of metabolite and the relative increase in fluorescence upon binding to the metabolite (fig. S2, table S1). Different transducer modules were found to be optimal for different sensors. For example, the optimal adenosine sensor contained a transducer comprising a stem with base pairs primarily composed of weaker A-U and G-U pairs (fig. S2A). In the case of the ADP and SAM sensors, shorter transducer modules with only 4 base pairs and 1 base pair, respectively, resulted in optimal metabolite-induced fluorescence (fig. S2B and C). The transducer modules for the guanine and GTP sensors were composed of truncated stems found in the parent aptamers (table S1).

Imaging ADP dynamics in *E. coli*. Most of the ~700 small molecule metabolites in microbial cells cannot be imaged in individual cells in real time in response to experimental treatments. Previous studies examined metabolite levels in samples that contained large numbers of bacterial cells, which provides an average measurement across a population. However, single-cell measurements of gene expression have revealed that isogenic microbial populations contain metabolically distinct subpopulations with distinct metabolic profiles (*5, 6*), which can account for metabolically distinct subpopulations which exhibit reduced antibiotic sensitivity (*7-9*). However, because of the lack of imaging tools, the dynamics and variability of the diverse metabolic pathways is largely unknown.

We examined the dynamics of ADP, an indicator of nutrient stress, which occurs when bacteria are unable to efficiently generate ATP from ADP (*10, 11*). We readily detected increases in ADP production when *E. coli* were switched to media containing carbon sources that were more difficult to use than glucose (fig. S7A and B). For example, when the media to acetate, a carbon source that induces nutrient stress because it requires activation of the glyoxylate bypass pathway (*12*), fluorescence levels rapidly rose, reaching a 1.8-fold increase over baseline levels within 30 min, and a ~6-fold increase by 3 hr (fig. S7A and B). The fluorescence increases correlate with increases in endogenous ADP levels as measured using a standard biochemical assay, indicating that fluorescence levels reflect the intracellular ADP concentration (fig. S7D). As a control, we examined the effects of experimental treatments on *E. coli* transformed with a Spinach-expressing plasmid. *E. coli* exhibited uniform levels of Spinach fluorescence (fig. S4A and B), indicating that this expression system produces equivalent levels of RNA aptamer expression in each cell, with no changes in fluorescence during any of the experimental treatments (fig. S5F). These data confirm that the changes in fluorescence seen in *E. coli* expressing the ADP sensor derive from differences in sensor fluorescence, rather than nonspecific effects on Spinach fluorescence.

Monitoring population dynamics of SAM synthesis. SAM levels in *E. coli* have not been studied on the single cell level, and variability in SAM levels has not previously been possible to address due to the absence of tools to image SAM. SAM is synthesized in cells from methionine and ATP by SAM synthase (*13*). Expression of the SAM sensor in *E. coli* was able to robustly report on SAM biosynthesis elicited by methionine treatment (fig. S4C). Under the same conditions, the increases in SAM levels measured by an HPLC assay (*14*) matched the increases in fluorescence, indicating that fluorescence levels linearly correlate with intracellular SAM concentrations (fig. S4D). Control cells expressing Spinach showed no change in fluorescence under the same experimental conditions (fig. S5F).

The considerable cell-to-cell variability in SAM levels (Fig. 1C, fig. S5A, fig. S6A, movie S1), which has not previously been described, contrasted with the relative homogeneity seen in ADP biosynthetic rates (see fig. S7A). Intracellular SAM levels are influenced by pathways that recycle SAH (*13*). Using selective inhibitors, we find that the SAM hydroxylase-dependent recycling pathway has a substantial role in SAM metabolism in *E. coli* (fig. S5B-E, S6B). Because imaging of SAM levels in individual *E. coli* was not previously possible, the existence of inter-cell variability and the role of SAH hydroxylase was not previously known.

Measurement of the endogenous expression level of the sensors was achieved by Northern blotting *E. coli* expressing either the SAM or ADP sensor, and using in vitro transcribed sensor RNA as standards. Using this approach, we measured the SAM sensor at ~13.5 μM and the ADP sensor at ~75 μM in cells. Importantly, the sensors are expressed at a concentration significantly below the endogenous concentration of these metabolites, making it unlikely that the sensors would sequester these compounds and affect their metabolism.

Using Spinach for developing sensors that bind a wide array of small molecule targets. The major limitation that has prevented intracellular imaging of most metabolites is the absence of metabolite-binding proteins that undergo conformational changes sufficient to affect FRET. In most cases proteins that bind target molecules of interest either have not been identified, or bind to target molecules but do not exhibit sufficiently large conformational changes. The sensors described here take advantage of two features of RNA aptamers to overcome these problems. First, RNA aptamers can be generated against virtually any target molecule (*15, 16*). Additionally, RNA aptamers can routinely be selected such that they exhibit high selectivity towards target molecules versus molecules that differ by as little as a methyl or phosphate group (*17, 18*). Selection techniques have been described so that the affinity of aptamers can be tuned to yield aptamers that bind target molecules with desired affinities, typically in the nanomolar or micromolar range (*15*). Second, RNA aptamers commonly transition from an unfolded to a folded state upon binding small molecule targets (*19*). The sensors described here take advantage of this mode of ligand binding to allosterically regulate Spinach fluorescence.

In cases where the cell has uneven morphology, normalizing sensor fluorescence to another plasmid-encoded fluorophore, such as red fluorescent protein, would ensure that changes in fluorescence signals are not due to local volume differences or cell-to-cell variation in sensor expression. An additional consideration in the design of the sensors is that the EC_{50} should be larger than the endogenous concentration of the metabolite in the cell. If the sensor is too sensitive, the sensor may be fully saturated at physiologic levels of the metabolite, and therefore unable to detect changes in metabolite levels. Tuning of the metabolite-binding aptamer using mutagenesis or selection techniques (*20, 21*), will be important to match the sensitivity of the sensor with the endogenous metabolite concentration.

A major aspect of these sensors is that they use DFHBI, which does not exhibit nonspecific fluorescence activation upon incubation with cells, making background fluorescence from the unbound fluorophore minimal. This is in contrast to other fluorophores that can be activated by aptamers, or fluorophores which bind metabolite-regulated aptamers, such as malachite green, Hoechst 65442, and cyanine dyes (*22-26*), which are more susceptible to nonspecific fluorescence upon incubation with cells or biological materials (*26-34*). DFHBI also has negligible phototoxicity (*32*), which along with its brightness and low background make Spinach-based sensors particularly useful for the design of genetically encoded sensors for imaging metabolites in living cells.

In our studies, we focused on detecting molecules in *E. coli*. It will be important to extend these sensors to other cell types including mammalian, yeast, and plant cells. In mammalian cells, aptamers can be restricted to the nucleus or be susceptible to intracellular degradation. Thus, nuclear export sequences and stabilizing elements will be required to maximize sensor expression levels in the cytosol in order to use these sensors for imaging in mammalian cells.

MATERIALS AND METHODS

Reagents and equipment

Unless otherwise stated, all reagents were purchased from Sigma-Aldrich. DFHBI was prepared as described previously (*32*) or from Lucerna Technologies (New York, NY). Commercially available reagents were used without further purification. HPLC assays were performed on an Agilent 1100 series HPLC with a Zorbax C8 column. Absorbance spectra were recorded with a Thermo Scientific NanoDrop 2000 spectrophotometer with cuvette capability. Fluorescence excitation and emission spectra were measured with a Perkin Elmer LS-55 fluorescence spectrometer.

EC_{50} measurements

Dose-response curves for each sensor in response to the target metabolite were determined by measuring the increase in fluorescence as a function of increasing target concentration in the presence of a fixed concentration of RNA sensor (10-50 nM) and a fixed concentration of fluorophore (10 μM). Curves were determined using a nonlinear regression analysis in Prism software and matched by least squares fitting to a standard dose-response model for 1:1 complexation.

Preparation of RNA sensors and mutants

Secondary structure prediction was performed using Mfold online software. Mutated and truncated RNAs were created by ordering single stranded DNA templates (Integrated DNA Technologies) with the desired mutations or truncations and PCR amplifying these sequences to create double stranded DNA templates using primers which included a 5’ T7 promoter sequence. PCR products were then purified with PCR purification columns (Qiagen) and used as templates for in vitro T7 transcription reactions (Epicentre).

Sensor activation and deactivation rates

A solution of RNA sensor (1 μM) and DFHBI (10 μM) was incubated with continuous stirring at 37^{o}C in a buffer containing 40 mM HEPES pH 7.4, 125 mM KCl and 1 mM $MgCl_2$. The target metabolite (1 mM) was then rapidly added to the stirring solutions and fluorescence emission was recorded over a 15 min period under continuous illumination at 37°C using the following instrumental parameters: excitation wavelength, 460 nm; emission wavelength, 500 nm; increment of data point collection, 0.05 s; slit widths, 10 nm. The fluorescence increase was then plotted against exposure time and normalized to the maximum intensity of each fluorophore.

To measure deactivation rates, a solution of RNA sensor (0.1 μM) and DFHBI (10 μM) was incubated with target metabolite (1 mM) in a buffer containing 40 mM HEPES pH 7.4, 125 mM KCl and 10 mM $MgCl_2$ at 37^{o}C. When sensors reached maximal fluorescence, the solution was transferred to a buffer-exchanged RNase-Free Micro Bio-Spin column (Bio-Rad) with Bio-Gel P-30 in the above buffer without metabolite, and spun at 1000 x g for 4 min. The fluorescence emission of flow through was then immediately recorded over a 20 min at 37°C using the following instrumental parameters: excitation wavelength, 460 nm; emission wavelength window, 480-600 nm; slit widths, 10 nm. The fluorescence decrease was then plotted against time and normalized to the maximum intensity of the sensor spun through a column containing 1 mM metabolite. The control experiment (buffer exchanged columns with buffer containing the metabolite) was performed at same time. The fluorescence of the control sample was not significantly affected by the spin and incubation process.

Cloning sensors for expression in *E. coli*.

ADP and SAM sensors were PCR amplified with primers containing either EagI or SacII restriction sites on the 5' or 3' ends of the sensor sequence, respectively. Sensors were then cloned into a plasmid containing a chimera of the human $\text{tRNA}^{\text{Lys}}{}_3$ scaffold, which has previously been shown to stabilize heterologous expression of RNA aptamers in *E. coli* (*35*) (A generous gift of F. Dardel [Université Paris Descartes]). The entire tRNA-sensor construct was then PCR amplified with a forward primer containing a BglII site (italics) and a T7 promoter sequence (bold): 5'-CAG TCA *AGA TCT* CGA TCC CGC GAA AT **TAA TAC GAC TCA CTA TAG GG**-3', and a reverse primer containing a XhoI site (italics) and a T7 terminator sequence (bold): 5'- CAT CAG *CTC GAG* **CAA AAA ACC CCT CAA GAC CCG TTT AGA GGC CCC AAG GGG TTA TGC TA**-3'. This PCR product was then cloned into a pET28c vector with BglII and XhoI restriction sites.

Sensor levels in *E. coli* were measured by Northern blot, using in vitro transcribed sensor RNA as standards for preparing a standard curve. Aliquots of RNA harvested from *E. coli* expressing the ADP or SAM sensor was prepared using acidic-phenol:$CHCl_3$ extraction as per the manufacturer's instructions (Ambion), and then quantified by Northern blotting using a biotinylated Spinach-specific probe. To calculate the concentration, the intracellular *E. coli* volume was considered 7×10^{-16} L, and the number of *E. coli* was measured by plating an aliquot of the cell suspension on LB plates.

Live cell imaging of ADP dynamics

BL21-A Star *E. coli* cells (Invitrogen) were transformed with 40 ng of plasmid DNA expressing the tRNA-sensor chimeras in pET28c under the control of a T7 promoter. Cells were plated, grown overnight and single colonies were picked for inoculation in Luria Broth containing kanamycin (LB-Kan). At OD_{600} = 0.4, 1 mM of IPTG was added to the culture and shaking was continued at 37°C for more 2 hours. 100 uL of culture was then removed, spun down to pelleted the culture, and resuspended in 2 mL of pH 6.0 M9 minimal media. A 200 μl aliquot of resuspended culture was then plated on poly-L-lysine (PLL)-coated 24-well glass-bottom dishes (MatTek) and incubated for 45 minutes at 37°C. Adherent cells were washed twice and then incubated with 200 μM DFHBI in pH 6.0 M9 minimal media for 45 min at 37°C. Cells then were washed twice and incubated with M9 media containing 200 μM DFHBI and the appropriate carbon source (2 mg/ml glucose, 6.65 mg/ml potassium acetate, 4.05 mg/ml glycerol or 5.51

mg/ml succinate). Live fluorescence images were taken with a CoolSnap HQ2 CCD camera through a 60X oil objective mounted on a Nikon TE2000 microscope and analyzed with the NIS-Elements software. The filter set used was a sputter coated filter cube with excitation filter 470/40, dichroic mirror 495 (long pass) and emission filter 525/50 (Chroma Technology).

Biochemical measurement of ADP levels

Cells transformed with ADP sensor were grown overnight in LB-Kan. Cultures were then diluted to OD_{600} = 0.1 in 200 mL LB-Kan and grown to OD_{600} = 0.4. Cells were then induced for 2 hours with 1 mM IPTG at 37°C with constant shaking. The entire culture was split in two samples and then placed in a centrifuged for 5 min at 1,000 x g. Pellets were then washed once and resuspended in 400 mL of M9 media containing 200 μM DFHBI and either 2.00 mg/ml glucose or 6.68 mg/ml potassium acetate as the carbon source. After a 2 hr incubation, cells incubated in glucose were switched a media containing acetate and cells incubated in acetate were switched to a media containing glucose. Aliquots of culture were removed every 30 min, pelleted, lysed, and ADP levels were measured with an ADP Fluorometric Assay Kit (Abcam) according to manufacturer's instructions.

Live cell imaging of SAM accumulation

Expression of the SAM aptamer and intracellular imaging was performed as described above for the ADP sensor: BL21-A Star *E. coli* cells (Invitrogen) were transformed with 40 ng of plasmid DNA expressing the tRNA-sensor chimeras in pET28c under the control of a T7 promoter. Cells were plated, grown overnight and single colonies were picked for inoculation in LB-Kan. At OD_{600} = 0.4, 1 mM of IPTG was added to the culture and shaking was continued at 37°C for more 2 hours. 100 μL of culture was then removed, spun down to pellet the culture, and resuspended in 2 mL of pH 6.0 M9 minimal media. A 200 μl aliquot of resuspended culture was then plated on PLL-coated 24-well glass-bottom dishes (MatTek) and incubated for 45 minutes at 37°C. Adherent cells were washed twice and then incubated with 200 μM DFHBI in pH 6.0 M9 minimal media for 2 hours at 37°C. Cells were then treated with methionine alone or methionine with inhibitors by adding 2 μl of a 100x stock of the compound to a final concentration of 50 μg/ml for L-methionine, 25 μM for adenosine periodate, and 2.5 μM for MT-DADMe-ImmA. Live fluorescence images were taken with a CoolSnap HQ2 CCD camera through a 60X oil objective mounted on a Nikon TE2000 microscope and analyzed with the NIS-Elements software. The filter set used was a sputter coated filter cube with excitation filter 470/40, dichroic mirror 495 (long pass) and emission filter 525/50 (Chroma Technology).

HPLC measurement of aggregate SAM levels

Cells transformed with SAM sensors were grown overnight in LB-Kan. Cultures were then diluted to OD_{600} = 0.1 in 200 mL LB-Kan and grown to OD_{600} = 0.4. Cells were then induced for 2 hours with 1 mM IPTG at 37°C with constant shaking. The entire culture was centrifuged for 5 min at 1,000 x g, pellets were resuspended and washed once with M9 media and then resuspended in 400 mL of M9 media containing 200 μM DFHBI and divided into two samples. Methionine (50 μg/ml) or vehicle was then added to either sample and cultures were incubated between 32-37^{o}C. 25 ml aliquots were removed from methionine- and vehicle-treated sample at each time point, centrifuged for 5 min at 1,000 x g, and flash frozen in liquid nitrogen. Cells were thawed on ice and lysed by resuspending the pellet in 300 μl of cold 4% perchloric acid. Insoluble material was then pelleted by spinning at 1,000 x g for 5 min and the supernatant was transferred to a dialysis spin column with a 10,000 molecular weight cut off (Amicon) and spun at 10,000 x g for 10 min at 4^{o}C. A portion of the flow through (50 μl) was then injected on a Zorbax C8 column (Agilent) on an Agilent 1100 HPLC. Samples were loaded and eluted for 15 min with an aqueous buffer containing 3.6% acetonitrile, 40 mM ammonium phosphate, and 5 mM sodium 1-heptanesulfonate which was brought to pH 5.0 with hydrochloric acid. After each sample was eluted, the column was washed with a gradient of 3.6-25% acetonitrile for 30 min prior to the next samples being injected. SAM standards were used to calibrate SAM levels measured using this assay.

Population analysis of SAM production

Population analysis was carried out using NIS-Elements software. Individual cells in a captured field were manually traced as Region of Interests (ROIs) and tracked through the different time points of image capture. Fluorescence intensity was then calculated by dividing the total fluorescence by the area for each ROI, which gives the mean intensity per unit area. Fold increase in fluorescence over time is calculated as the ratio of mean intensity at a desired time point and at time zero. Values in fold increase in fluorescence over time are plotted as frequency distributions or further used in statistical analyses.

Levene Test for Equality of Variances

Levene tests for equality of variances were conducted using the Microsoft Excel QI Macros 2011 plug-in.

SUPPLEMENTARY FIGURE AND MOVIE LEGENDS

Figure S1. Identification of an insertion point on spinach RNA.

(A) Sequence of the SELEX library used to select for Spinach (DFHBI-binding) RNA aptamers. The library that was originally used to generate Spinach was composed of two 26-nucleotide long randomized domains flanking a central highly stable 12-base stem-loop structure (boxed in blue)., composed of a 4-base pair stem and a stable UUCG tetraloop (fig. S1A and B) (*32, 36*). This stem-loop structure eventually became stem-loop 2 in the final Spinach sequence. Because stem-loop 2 was a fixed sequence in every library member, it may be less likely to make sequence-specific contacts with DFHBI, and more likely to have a structural role in DFHBI binding that could be exploited in sensor design. For this reason, we inserted this sequence in the library in order to have a stem-loop that would be poised to have a structural role in Spinach. If Spinach-induced DFHBI fluorescence is dependent on the structure of this stem-loop, then sensors which allosterically regulate the formation of the stem would activate fluorescence.

(B) The predicted secondary structure of a minimized Spinach sequence with stem-loops 1, 2 and 3 indicated by a blue box. The structure was generated using Mfold. Previous experiments have indicated that stem-loop 1 and 3 of Spinach are critical to Spinach-induced fluorescence. Mutations of nucleotides in the loops, as well as structure-preserving mutations in these stems significantly impaired Spinach-induced DFHBI fluorescence (*32*). Thus these stem-loops appear to have sequence-specific roles in inducing DFHBI fluorescence. However, the role of stem-loop 2 in Spinach-induced DFHBI fluorescence was not previously examined.

(C) Stem-loop 2 has a structural role in Spinach-induced DFHBI fluorescence. Stem-loop substitutions were used to test the adaptability of Spinach for sensors. In these experiments we used a minimized Spinach structure in which stem-loop 2 is predicted to sit adjacent to the large internal loop (fig. S1B). This minimized Spinach sequence exhibits essentially identical fluorescence as the full length Spinach sequence (*32*). Stem-loops were inserted into Spinach at the position of stem-loop 2 in Fig. 1A. Stem-loop 2 is the original fixed sequence from the library used to select for Spinach. The "replacement stem-loop" differs completely in sequence to stem-loop 2 but retains a similar structure. In this stem-loop, we replaced the UUCG loop sequence with GAAA and replaced the 4-base pair stem with a different but still complementary 4-basepair stem. The "mismatched stem" retains the original UUCG tetraloop found in Spinach, but replaces the stem with three mismatched nucleotides to prevent duplex formation.

(D) DFHBI fluorescence in the presence of three different stem-loop insertions in Spinach. Stem-loop 2 and the replacement stem-loop have nearly identical fluorescence intensities even though they are completely unrelated sequences. However, the mismatched stem reduces fluorescence intensity to baseline even though it retains the original UUCG tetraloop. This indicates that Spinach is amenable to changes in the sequence at the position of stem-loop 2; however, rigidification at the stem portion is necessary for fluorescence activation of DFHBI.

(E) Schematic of DFHBI binding to Spinach. The Spinach RNA aptamer is capable of binding to and activating the fluorescence of the small molecule fluorophore DFHBI (green circle). In the unbound form, DFHBI is completely nonfluorescent, but becomes robustly fluorescent upon binding to Spinach. DFHBI is designed to mimic the fluorescence properties of EGFP. DFHBI fluorescence activation by Spinach requires the formation of a duplexed stem in stem-loop 2 (boxed in blue).

(F) Modular design of Spinach-based sensors. We constructed Spinach-based sensors using a modular approach comprising: (1) a recognition module which constitutes a metabolite-binding aptamer, (2) a transducer module that has an essential structural role in stabilizing Spinach and "transmits" the metabolite binding event, and (3) a Spinach module. The transducer module is composed of two strands which form a weakly basepaired stem. Folding of the recognition domain provides additional stability that facilitates the hybridization of the stem region in the recognition module. The Spinach module binds to and activates the fluorescence of DFHBI, but only when the transducer module forms a stem. This approach of using small molecules to allosterically regulate RNA structure has been used to develop small molecule-regulated ribozymes and aptamers (*37-40*), and these RNA devices have been shown to undergo structural rearrangements upon ligand binding which serves to increase ribozyme or other activities (*41, 42*).

Figure S2. Optimization of stem transducer modules for adenosine, ADP and SAM sensors.

(A) Spinach RNA was produced in which stem-loop 2 was replaced with an aptamer to adenosine. The adenosine aptamer was fused to Spinach by one of seven different transducer modules. These transducer modules contained different combination of G-C, A-U and G-U base pairs, and were chosen because they were predicted to have a very low probability of duplex formation using the prediction software Mfold. Adenosine sensors containing different stems (stem 1-7) were incubated with 10 μM DFHBI in the presence or absence of 1 mM adenosine, and fluorescence emission was measured. The optimal transducer module (stem 2) was chosen because in the context of the sensor it displayed low background fluorescence, with a 20-fold increase in fluorescence signal upon incubation with adenosine. Stem 2 contained primarily A-U and G-U base pairs with G-C pairs only at the ends of the stem.

(B) Spinach-based sensors to ADP were produced with different transducer modules (stem 1-8) as described above for adenosine sensors. ADP sensor transducer modules contained different combination of G-C, A-U and G-U base pairs, and were chosen because they were predicted to have a very low probability of duplex formation using the prediction software Mfold. ADP sensor variants were tested as described for the adenosine sensors, and an optimal transducer module (stem 3) with a 20-fold increase in fluorescence was identified.

(C) Spinach-based sensors to SAM were produced with different transducer modules (stem 1-10) as described above for adenosine and ADP sensors. SAM sensor transducer modules contained different lengths and combinations of G-C, A-U and G-U base pairs. Longer stems in the transducer module lead to increased fluorescence in the absence of SAM. The optimal transducer module contained only a single G-C base pair (stem 1), which was positioned adjacent to the SAM binding site. This sensor has a 25-fold increase in fluorescence upon SAM binding and exhibited the lowest background signal.

Figure S3. Dose-response, specificity and kinetics experiments for RNA sensors

(A) Emission spectra of the RNA sensor for adenosine (Ade) in the presence or absence of Ade. Spectra were collected at 0.1 μM RNA, 10 μM DFHBI and 1 mM Ade. Fluorescence signal is negligible in the absence of Ade and increases 16-fold in the presence of Ade.

(B) Emission spectra of the RNA sensor for ADP in the presence or absence of ADP. Spectra were collected at 0.1 μM RNA, 10 μM DFHBI and 1 mM ADP. Fluorescence signal is negligible in the absence of ADP and increases 18-fold in the presence of ADP.

(C) Emission spectra of the RNA sensor for guanine (Gua) in the presence or absence of Gua. Spectra were collected at 0.1 μM RNA, 10 μM DFHBI and 100 μM Gua. Fluorescence signal is negligible in the absence of Gua and increases 32-fold in the presence of Gua.

(D) Emission spectra of the RNA sensor for GTP in the presence or absence of GTP. Spectra were collected at 0.1 μM RNA, 10 μM DFHBI and 1 mM GTP. Fluorescence signal is negligible in the absence of GTP and increases 15-fold in the presence of GTP.

(E) Dose-response curve for fluorescence detection of adenosine by the RNA-based sensor to adenosine. Half-maximal fluorescence is reached at 44 μM adenosine.

(F) Dose-response curve for fluorescence detection of ADP by the ADP RNA sensor. Half-maximal fluorescence is reached at 270 μM ADP.

(G) Dose-response curve for fluorescence detection of guanine by the RNA-based guanine sensor. Half-maximal fluorescence is reached at 1.5 μM guanine. The guanine sensor was highly sensitive and displayed an EC_{50} lower than the concentration of guanine in cells (*43*).

(H) Dose-response curve for fluorescence detection of GTP by the RNA-based sensor to GTP. Curve fitting predicted that half-maximal fluorescence is reached at 7.7 mM GTP.

(I) Dose-response curve for fluorescence detection of SAM by the SAM RNA sensor. Half-maximal fluorescence is reached at 120 μM SAM.

(J) Molecular discrimination of adenosine sensor. 0.1 μM RNA and 10 μM DFHBI were incubated with 1 mM adenosine or competing molecules and assayed for fluorescence emission at 500 nm. The adenosine sensor is highly specific for adenosine over other nucleosides and adenosine 3'-phosphorylated nucleotides, but also fluoresces in the presence of adenosine 5'-phosphorylated-nucleotides, such as ADP and ATP, which is consistent with the known binding specificity of the parent aptamer (*1*). However, the sensor is specific for adenosine over the 3'-phosphorylated adenosine derivative cAMP. The adenosine sensor also shows negligible fluorescence in the presence of guanine-containing nucleosides (guanosine) and nucleotides (GTP).

(K) Molecular discrimination of the ADP sensor. The ADP sensor is specific for ADP over other highly similar adenosine-containing nucleotides including ATP, AMP, cAMP and NAD^+. The ADP sensor remains selective even at very high concentrations (1 mM) of competing molecules.

(L) Molecular discrimination of the guanine sensor. The guanine sensor saturates at 100 μM guanine, and shows a high level of molecular discrimination against guanosine and adenine at the same concentrations. 0.1 μM RNA and 10 μM DFHBI were incubated with 100 μM guanine or competing molecules and assayed for fluorescence emission at 500 nm. guanosine. Only baseline fluorescence is seen in the presence of guanosine or adenine.

(M) Molecular discrimination of the GTP sensor. 0.1 μM RNA and 10 μM DFHBI were incubated with 1 mM GTP or competing molecules and assayed for fluorescence emission at 500 nm. The GTP sensor exhibits moderate preference for GTP over GMP, suggesting that this sensor could be mutagenized and re-selected to be more specific for GTP over other 5'-phosphorylated derivatives, such as GDP and GMP. The GTP sensor exhibits tenfold less fluorescence in the presence of the 3'-phosphorylated derivative cGMP and the unphosphorylated nucleoside guanosine. Only baseline fluorescence is seen in the presence of ATP.

(N) Molecular discrimination of the SAM sensor. The SAM sensor shows a high level of molecular discrimination against highly related molecules. The SAM sensor shows only minimal fluorescence with 1 mM *S*-adenosylhomocysteine (SAH), the byproduct of SAM-dependent methyltransferases, which differs from SAM by only a single methyl group. The intracellular concentration of SAH is several orders of magnitude below this level (*43*). SAM precursors adenosine gave negligible signal above background at 1 mM.

(O) Measurement of rate of SAM sensor activation. We next measured the rate of fluorescence activation following metabolite addition. Addition of either SAM or ADP resulted in increases in fluorescence in less than 10 s, with maximal levels of fluorescence within ~10 min. A solution of RNA sensor (1 μM) and DFHBI (10 μM) was incubated with continuous stirring at 37^{o}C in a buffer containing 40 mM HEPES pH 7.4, 125 mM KCl and 1 mM $MgCl_2$. SAM (1 mM) was then rapidly added to the stirring solutions and fluorescence emission was recorded over a 15 min period under continuous illumination at 37°C using the following instrument parameters: excitation wavelength, 460 nm; emission wavelength, 500 nm; increment of data point collection, 0.05 s; slit widths, 10 nm. The fluorescence increase was then plotted against exposure time and normalized to the maximum intensity. The measured activation and deactivation rates are highly sensitive to ionic and temperature conditions.

(P) Measurement of rate of ADP sensor activation. A solution of RNA sensor (1 μM) and DFHBI (10 μM) was incubated with continuous stirring at 37^{o}C in a buffer containing 40 mM HEPES pH 7.4, 125 mM KCl and 1 mM $MgCl_2$. ADP (1 mM) was added to the stirring solutions and fluorescence emission was recorded over a 15 min period under continuous illumination at 37°C using the following instrument parameters: excitation wavelength, 460 nm; emission wavelength, 500 nm; increment of data point collection, 0.05 s; slit widths, 10 nm. The fluorescence increase was then plotted against exposure time and normalized to the maximum intensity. ADP sensors reach maximal fluorescence within 12 min.

(Q) Measurement of rate of SAM sensor deactivation. The goal of this experiment was to determine how quickly the SAM sensor fluorescence is lost once SAM is removed from the sensor. We used a gel filtration spin column to remove the sensor. Conditions to measure deactivation were similar to the activation experiments as described in the Methods. SAM sensor fluorescence was deactivated by >90% within 10 min.

(R) Measurement of rate of ADP sensor deactivation. The goal of this experiment was to determine how quickly the ADP sensor fluorescence is lost once ADP is removed from the sensor. We used a gel filtration spin column to remove the sensor. Conditions to measure deactivation were similar to the activation experiments as described in the Methods. ADP sensor fluorescence was deactivated by >90% within 8 min. The relatively rapid deactivation rates of the SAM and ADP sensors suggests that these sensors can faithfully respond to changes in intracellular SAM and ADP in cells.

Figure S4. Demonstration of uniform Spinach expression in *E. coli* and variability of endogenous SAM levels.

(A) Spinach-expressing *E. coli* demonstrate uniformity in RNA expression level. Phase and fluorescence image of *E. coli* transformed with a plasmid expressing Spinach RNA. Spinach-expressing cells were imaged under microscope settings where fluorescence was non-saturated and the level of fluorescence signal was quantified per cell. Cells exhibited highly uniform levels of fluorescence throughout the population demonstrating that this expression system produces very little cell-to-cell variation in heterologous RNA expression levels.

(B) Quantification of fluorescence signal from Spinach-expressing cells in a population to test uniformity in RNA expression levels. Spinach fluorescence levels were quantified per cell and the number of cells with a given fluorescence intensity were plotted as percentage change for the mean fluorescence calculated from the entire population. 150 cells were counted across three experimental replicates. The large majority of cells exhibited Spinach fluorescence signal within +/-10% of mean fluorescence for the entire population of cells.

(C) The SAM sensor detects changes in endogenous SAM levels in living cells. *E. coli* expressing the SAM sensor were briefly cultured in methionine-free media and then were treated with either 25 μM methionine or vehicle and imaged continuously for 3 hr. Images of cells 0 min and 180 min after treatment are shown. SAM levels increased an average of six-fold upon treatment with methionine (a precursor in SAM synthesis) whereas vehicle-treated cells showed only minimal increases in SAM levels. Scale bar, 5 µm.

(D) Increases in SAM fluorescence correlate with biochemical measurements of SAM. SAM sensors can accurately measure increases in endogenous SAM levels. SAM sensor-expressing cells were treated with 50 μg/ml methionine (+met) or vehicle (-met) for 3 hr and fluorescence increases were measured in single living cells by epifluorescence microscopy. Cells treated identically were also lysed at different time points and total SAM levels were measured by an HPLC assay. Average fluorescence increase was plotted against HPLC data. SAM RNA sensors accurately measure increases in SAM levels and correlate with HPLC data. For fluorescence measurements, 300 cells were quantified for each condition over three experimental replicates. For HPLC measurements, the average value from three experimental replicates is plotted. Error bars represent the standard error of the mean.

(E,F) Variability in SAM accumulation revealed by single cell imaging can be categorized into four distinct types. Briefly, SAM sensor fluorescence signals of 100 cells from two independent experiments were analyzed. Obvious patterns in intracellular SAM increase such as exponential increase (signal rise over time fitted an exponential function curve) or peak (signal rose to a maximum then dropped) were categorized as Exponential Response or Peak Response. Overall rate of increase in intracellular SAM was calculated for individual cells and tabulated. Cells whose rates of increase are within two standard deviations of the mean are characterized as Normal Response. Cells whose rates of increase are two standard deviations higher than the mean were counted as Fast Response. The fluorescence levels of the SAM sensor were plotted over time. Representative examples of the fluorescence in live cells (in false color) showing each of the four categories are also shown. The majority of cells exhibited a continuous increase in SAM levels over the 3 hr time course of methionine treatment, and this increase in SAM levels was labeled as "normal response". However, a small percentage (~4%) of cells briefly increased to a peak SAM level and then rapidly decreased their intracellular SAM levels to baseline levels. This increase followed by a decrease was labeled as "peak response". Other cells exhibited a more rapid or even exponential increase in SAM levels. These responses were labeled "fast response" or "exponential response", and were exhibited by approximately 7% and 3% of the population, respectively (see fig. S4G for presentation of the quantification of the different SAM behavior subtypes).

(G) A quantification of the four types of increase in intracellular SAM levels showed the majority (86%) of the cell to be in the Normal Response category while the rest fell into one of three categories Fast, Peak or Exponential Response designating 7%, 4% and 3% of the sample cell population respectively.

Figure S5. Population dynamics of SAM accumulation and recycling pathways in living cells and analysis of Spinach-expressing *E. coli* showing that various treatments do not influence Spinach fluorescence

(A) Variability in SAM accumulation revealed by single cell measurements of intracellular SAM levels. *E. coli* were prepared as in (Fig. 1C) and total SAM sensor fluorescence was quantified per cell every 15 min following methionine treatment. Single cell measurements of the fold increase in fluorescence relative to the t=0 time point reveal large variations in SAM levels in different cells across the entire population. This fold increase in variance of the population increases from 30 min to 180 min, indicating that the population becomes more diverse at each time point throughout the 3 hr time course. The variance between SAM levels in the population increased over 20-fold from 30 min to 3 hr after methionine treatment. Values are reported as fold increase in fluorescence from values immediately after methionine treatment, and the percentage of cells in the population displaying a given fold increase in SAM are plotted. A total of 800 cells per time point were quantified from three experimental replicates.

(B-E) SAM recycling pathways influence SAM levels and variability in SAM accumulation in the population. Cells expressing the SAM sensor were briefly methionine starved and then incubated with 50 μg/ml methionine together with either vehicle, an SAH hydrolase inhibitor (Ado-2',3'-dial), or an SAH nucleosidase inhibitor (MT-DADMe-ImmA). *E. coli* treated with methionine in combination with the SAH hydrolase inhibitor adenosine-2',3'-dialdehyde (Ado-2',3'-dial) (*44, 45*), showed only a slight decrease in the average SAM levels at each time point compared to populations treated with methionine in combination with vehicle (fig. S5B-E, S6B). However, Ade-2',3'-dial-treated cells exhibited markedly reduced inter-cell variability in SAM levels compared to vehicle-treated cells at each time point (fig. S5B-E, S6B). This difference was most noticeable 1 hr after methionine treatment and then began to lessen by 2 hr after treatment (fig. S5B-E, S6B). In contrast, populations treated with the SAH nucleosidase inhibitor, MT-DADMe-Immucillin-A (MT-DADMe-ImmA) (*46*), showed a larger decrease in the average accumulation of SAM in cells compared to vehicle-treated populations, but retained considerable variability in total SAM levels at all time points (fig. S5B-E, S6B). These data indicate that SAH hydrolase and SAH nucleosidase have different roles in influencing the variability in SAM metabolism in *E. coli*, with SAH hydrolase contributing to the SAM variability seen in cells.

(F) In this experiment, we wanted to confirm that our experimental treatments were not having nonspecific effects on Spinach fluorescence. Cells were transformed with a Spinach-expressing plasmid, induced with IPTG, and prepared for microscopy using the same protocol described for sensor-expressing cells. Cells were then exposed to the same experimental treatments as the ADP or SAM sensor-expressing cells in Figs. 3-4 to determine if any of the treatments had an effect on Spinach fluorescence. To control for experiments using the ADP sensor, cells were incubated for 2 hr in glucose-containing media (or acetate-containing media) and then switched to acetate-containing media (or glucose-containing media) and fluorescence was recorded with an epifluorescence microscope for 3 hr. To control for experiments using the SAM sensor, cells were treated with L-methionine (50 μg/ml) alone, L-methionine with 25 μM adenosine periodate (Ado-2',3'-dial), or L-methionine with 2.5 μM MT-DADMe-ImmA. Fluorescence was recorded for 3 hr after treatments. Values are reported for times 0, 60, 120, and 180 min after treatment. Values are normalized to Spinach-expressing cells which received no treatment under identical imaging conditions. None of the treatments resulted in decreased Spinach signal compared to untreated cells.

Figure S6. Cumulative percentage frequency distribution plots to test for non-Gaussian distribution and population analysis of SAM accumulation under different treatment conditions.

(A) Experiments measuring the fold increase in SAM upon methionine treatment were quantified as in Figure 3B and a cumulative percentage frequency distribution analysis was performed to determine if the distribution of values was Gaussian. To do this, fold increase values were tabulated as percentages and plotted on a cumulative probability axis. A linear curve would indicate sampling from a Gaussian/normal distribution. Deviation from linearity implies non-normality and necessitates employment of subsequent statistical tests with the relevant non-normality compatibility and assumptions. Data from four different time points are shown, and all displayed non-linear curves showing non-Gaussian distributions.

(B) Population analysis of SAM accumulation under different treatments. Inhibition of different SAM recycling pathways causes distinct changes in SAM levels and population variance. Cells transformed with plasmids expressing the SAM sensor RNA were briefly methionine starved and then incubated with methionine (50 μg/ml) alone or with an SAH hydrolase inhibitor (Ado-2',3'-dial) or an SAH nucleosidase inhibitor (MT-DADMe-ImmA). Treatment with Ado-2',3'-dial resulted in very little change in the average SAM accumulation per cell over time, but did result in a significant reduction in the variability in SAM levels seen across the entire population. Treatment with Mt-DADMe-ImmA, on the other hand, resulted in a much greater reduction in average SAM accumulation levels, but actually increased the variability in SAM levels seen across the population.

Figure S7. Live cell imaging and biochemical confirmation of endogenous ADP levels.

(A) Spinach-based ADP sensors can detect changes in endogenous ADP levels in living cells. *E. coli* cells transformed with plasmids expressing the ADP sensor and grown in media containing 200 μM DFHBI and glucose were switched to a media containing a different carbon source. Fluorescence was imaged continuously with an epifluorescence microscope for 180 min. Phase images and fluorescence images at 0 min and 180 min after the media switch are shown. Cells switched from glucose-containing media to glucose (control), glycerol or succinate-containing media showed only a slight increase in ADP levels after 180 min of incubation while cells switched to acetate-containing media show much higher levels of ADP after the 180 min incubation. Cells transformed with a plasmid expressing a control aptamer were not fluorescent under identical imaging conditions. Under these conditions, *E. coli* transformed with a plasmid expressing a control RNA exhibited negligible fluorescence, confirming that fluorescence in these cells derives from the sensor. Scale bar, 5 µm.

(B) Quantification of fluorescence in cells expressing the ADP sensor after cells are switched from glucose-containing media to media containing different carbon sources. Individual cells were imaged over 3 hr and fluorescence was measured and normalized to the cellular area to quantify the cellular ADP level. Changing from a glucose-containing media to acetate resulted in the largest increases in fluorescence, while switching to other carbon sources produces more subtle increases in fluorescence levels. A total of 150 cells were quantified over three experimental replicates for each condition, and values shown are the average +/- standard error of the mean.

(C) Quantification of ADP levels when cells are switched from acetate-containing media to glucose-containing media. We next asked whether nutrient-starved *E. coli* rapidly readjust their metabolic state when switched to glucose-containing media. To test this, *E. coli* were cultured in 6.6 mg/ml potassium acetate for 2 hr, resulting in nutrient stress, as seen by the high baseline levels of ADP (fig. S7C). The media was then exchanged with media containing 2 mg/ml glucose as the sole carbon source. After treating *E. coli* with glucose, ADP levels dropped 74% within 30 min, indicating that nutrient-limited *E. coli* rapidly readjust their metabolism to utilize glucose. Interestingly, after the drop in ADP levels, the levels began to slowly rise after 30 min, and gradually level out after 2.5 hr, indicating a readjustment to a new metabolic state after the initial introduction of glucose. Importantly, the trends we observed are consistent with previous biochemical measurement of changes in ADP levels in *E. coli* following similar experimental treatments (*11*). Together, these data indicate that dynamic changes in intracellular ADP levels can be monitored using an RNA-based sensor. Values reported are an average from a total of 150 quantified cells, and error bars represent the standard error of the mean.

(D) Biochemical validation of the ADP levels measured in the fluorescence assay. The goal of this experiment was to see if the ADP levels measured by a biochemical assay (fluorometric ADP assay kit) matched the levels reported by the sensor. Bacterial cultures transformed with a plasmid expressing the ADP sensor were grown overnight in LB, induced with IPTG, and incubated with DFHBI in minimal media with glucose as the carbon source as in microscopy experiments. Under these conditions, cellular ADP levels are expected to be low. Cells were then switched to a media containing either glucose, acetate, succinate or glycerol as the carbon source. After 2 hr, cells were lysed and ADP levels were measured with a commercially available fluorimetric assay kit for ADP levels. ADP levels increased much more in cells switched to acetate-containing media than in cells that were switched to a media containing one of the other carbon sources. These results are consistent with the changes in ADP levels seen with the ADP sensor.

SUPPLEMENTARY MOVIE LEGEND

Movie S1. Variation in the rate of SAM accumulation across a population of *E. coli* cells.

SAM measurements with an RNA sensor to SAM reveal distinct patterns of SAM accumulation in individual cells. *E. coli* expressing the SAM sensor were briefly starved of methionine in minimal media and then incubated with 200 μM DFHBI and 50 μg/ml methionine to induce SAM synthesis. Images were recorded every 15 min for 180 min. Cells are pseudocolored to show the fold increase in SAM accumulation, relative to the 0 min timepoint, over the course of the experiment with blue being the lowest and red being the highest. Although many cells exhibit continuous increases in SAM levels at each subsequent time point, some cells appear to increase and then decrease their levels of intracellular SAM.

REFERENCES FOR SUPPLEMENTARY MATERIAL

1. M. Sassanfar, J. W. Szostak, An RNA motif that binds ATP. *Nature* **364**, 550 (1993).
2. C. Lu *et al.*, Crystal structures of the SAM-III/SMK riboswitch reveal the SAM-dependent translation inhibition mechanism. *Nat. Struct. Mol. Bio.* **15**, 1076 (2008).
3. R. T. Batey, S. D. Gilbert, R. K. Montange, Structure of a natural guanine-responsive riboswitch complexed with the metabolite hypoxanthine. *Nature* **432**, 411 (2004).
4. J. M. Carothers, S. C. Oestreich, J. H. Davis, J. W. Szostak, Informational complexity and functional activity of RNA structures. *J. Am. Chem. Soc.* **126**, 5130 (2004).
5. E. M. Ozbudak, M. Thattai, H. N. Lim, B. I. Shraiman, A. Van Oudenaarden, Multistability in the lactose utilization network of Escherichia coli. *Nature* **427**, 737 (2004).
6. M. Acar, A. Becskei, A. Van Oudenaarden, Enhancement of cellular memory by reducing stochastic transitions. *Nature* **435**, 228 (2005).
7. K. Lewis, Persister cells. *Annu. Rev. Microbiol.* **64**, 357 (2010).
8. M. Heinemann, R. Zenobi, Single cell metabolomics. *Curr. Opin. Biotechnol.* **22**, 26 (2011).
9. N. Q. Balaban, J. Merrin, R. Chait, L. Kowalik, S. Leibler, Bacterial persistence as a phenotypic switch. *Science* **305**, 1622 (2004).
10. M. H. Buckstein, J. He, H. Rubin, Characterization of nucleotide pools as a function of physiological state in Escherichia coli. *J. Bacteriol.* **190**, 718 (2008).
11. O. H. Lowry, J. Carter, J. B. Ward, L. Glaser, The effect of carbon and nitrogen sources on the level of metabolic intermediates in Escherichia coli. *J. Biol. Chem.* **246**, 6511 (1971).
12. A. J. Cozzone, Regulation of acetate metabolism by protein phosphorylation in enteric bacteria. *Annu. Rev. Microbiol.* **52**, 127 (1998).
13. S. C. Lu, S-Adenosylmethionine. *Int. J. Bioch. Cell Biol.* **32**, 391 (2000).
14. S. Merali, D. Vargas, M. Franklin, A. B. Clarkson, S-adenosylmethionine and Pneumocystis carinii. *J. Biol. Chem.* **275**, 14958 (2000).
15. R. Stoltenburg, C. Reinemann, B. Strehlitz, SELEX--a (r)evolutionary method to generate high-affinity nucleic acid ligands. *Biomol. Eng.* **24**, 381 (2007).
16. E. J. Cho, J.-W. Lee, A. D. Ellington, Applications of Aptamers as Sensors. *Annu. Rev. Anal. Chem.* **2**, 241 (2009).
17. P. L. Sazani, R. Larralde, J. W. Szostak, A small aptamer with strong and specific recognition of the triphosphate of ATP. *J. Am. Chem. Soc.* **126**, 8370 (2004).
18. R. D. Jenison, S. C. Gill, A. Pardi, B. Polisky, High-resolution molecular discrimination by RNA. *Science* **263**, 1425 (1994).
19. T. Hermann, D. J. Patel, Adaptive recognition by nucleic acid aptamers. *Science* **287**, 820 (2000).
20. G. A. Soukup, E. C. DeRose, M. Koizumi, R. R. Breaker, Generating new ligand-binding RNAs by affinity maturation and disintegration of allosteric ribozymes. *RNA* **7**, 524 (2001).
21. Z. Huang, J. W. Szostak, Evolution of aptamers with a new specificity and new secondary structures from an ATP aptamer. *RNA* **9**, 1456 (2003).
22. C. Furutani, K. Shinomiya, Y. Aoyama, K. Yamada, S. Sando, Modular blue fluorescent RNA sensors for label-free detection of target molecules. *Mol. BioSyst.* **6**, 1569 (2010).
23. M. N. Stojanovic, D. M. Kolpashchikov, Modular aptameric sensors. *J. Am. Chem. Soc.* **126**, 9266 (2004).
24. S. Sando, A. Narita, M. Hayami, Y. Aoyama, Transcription monitoring using fused RNA with a dye-binding light-up aptamer as a tag: a blue fluorescent RNA. *Chem. Comm.*, 3858 (2008).
25. J. Babendure, S. Adams, R. Tsien, Aptamers switch on fluorescence of triphenylmethane dyes. *J. Am. Chem. Soc.* **125**, 14716 (2003).

26. T. P. Constantin *et al.*, Synthesis of new fluorogenic cyanine dyes and incorporation into RNA fluoromodules. *Org. Lett.* **10**, 1561 (2008).
27. E. Ippen, C. Shank, A. Bergman, Picosecond recovery dynamics of malachite green. *Chem. Phys. Lett.* **38**, 611 (1976).
28. S. Kim, G. Fleming, Reorientation and isomerization of trans-stilbene in alkane solutions. *J. Phys. Chem.* **92**, 2168 (1988).
29. T. Nagele, R. Hoche, W. Zinth, J. Wachtveitl, Femtosecond photoisomerization of cis-azobenzene. *Chem. Phys. Lett.* **272**, 489 (1997).
30. R. Sension, S. Repinec, A. Szarka, R. Hochstrasser, Femtosecond laser studies of the cis-stilbene photoisomerization reactions. *J. Chem. Phys.* **98**, 6291 (1993).
31. V. Sundstrom, T. Gillbro, Viscosity-dependent isomerization yields of some cyanine dyes - a picosecond laser spectroscopy study. *J. Phys. Chem.* **86**, 1788 (1982).
32. J. S. Paige, K. Y. Wu, S. R. Jaffrey, RNA mimics of green fluroescent protein. *Science* **333**, 642 (2011).
33. C. Dugave, L. Demange, Cis-trans isomerization of organic molecules and biomolecules: Implications and applications. *Chem. Rev.* **103**, 2475 (2003).
34. S. Meech, Excited state reactions in fluorescent proteins. *Chem. Soc. Rev.*, (2009).
35. L. Ponchon, F. Dardel, Recombinant RNA technology: the tRNA scaffold. *Nat. Methods* **4**, 571 (2007).
36. J. Davis, J. Szostak, Isolation of high-affinity GTP aptamers from partially structured RNA libraries. *Proc. Natl. Acad. Sci. U.S.A.* **99**, 11616 (2002).
37. J. Tang, R. Breaker, Rational design of allosteric ribozymes. *Chem. Biol.* **4**, 453 (1997).
38. J. Tang, R. R. Breaker, Mechanism for allosteric inhibition of an ATP-sensitive ribozyme. *Nucleic Acids Res.* **26**, 4214 (1998).
39. G. A. Soukup, R. R. Breaker, Design of allosteric hammerhead ribozymes activated by ligand-induced structure stabilization. *Structure* **7**, 783 (1999).
40. M. N. Win, C. D. Smolke, Higher-order cellular information processing with synthetic RNA devices. *Science* **322**, 456 (2008).
41. M. N. Win, J. C. Liang, C. D. Smolke, Frameworks for programming biological function through RNA parts and devices. *Chem. Biol.* **16**, 298 (2009).
42. A. R. Buskirk, A. Landrigan, D. R. Liu, Engineering a ligand-dependent RNA transcriptional activator. *Chem. Biol.* **11**, 1157 (2004).
43. B. D. Bennett *et al.*, Absolute metabolite concentrations and implied enzyme active site occupancy in Escherichia coli. *Nat. Chem. Biol.* **5**, 593 (2009).
44. J. X. Wang, E. R. Lee, D. R. Morales, J. Lim, R. R. Breaker, Riboswitches that sense S-adenosylhomocysteine and activate genes involved in coenzyme recycling. *Mol. Cell* **29**, 691 (2008).
45. M. Hermes, H. Osswald, J. Mattar, D. Kloor, Influence of an altered methylation potential on mRNA methylation and gene expression in HepG2 cells. *Exp. Cell Res.* **294**, 325 (2004).
46. J. A. Gutierrez *et al.*, Transition state analogs of 5'-methylthioadenosine nucleosidase disrupt quorum sensing. *Nat. Chem. Biol.* **5**, 251 (2009).

Table S1. Sequences for RNA-based small molecule sensors.

Target Metabolite	RNA sensor sequence*
Adenosine	**GACGCGACTGAATGAAATGGTGAAGGACGGGTCCA** *GTAATGGGAAGAAACTGTGGCACTTCGGTGCCAGCGTTGC* **TTGTTGAGTAGAGTGTGAGCTCCGTAACTAGTCGCGTC**
ADP	**GACGCGACTGAATGAAATGGTGAAGGACGGGTCCA** *GCACGAGGGGGAAACCCCGGACAATCAGACACGGTGC* **TTGTTGAGTAGAGTGTGAGCTCCGTAACTAGTCGCGTC**
SAM	**GACGCGACTGAATGAAATGGTGAAGGACGGGTCCA** *CGAAAGGATGGCGGAAACGCCAGATGCCTTGTAACCGAAAGGG* **TTGTTGAGTAGAGTGTGAGCTCCGTAACTAGTCGCGTC**
Guanine	**GACGCGACTGAATGAAATGGTGAAGGACGGGTCCA** *GATAATCGCGTGGATATGGCACGCAAGTTTCTACCGGGCACCGTAAATGTCCGACTC* **TTGTTGAGTAGAGTGTGAGCTCCGTAACTAGTCGCGTC**
GTP	**GACGCGACTGAATGAAATGGTGAAGGACGGGTCCA** *GCAGAAGAGCACGTATACGCAAGC* **TTGTTGAGTAGAGTGTGAGCTCCGTAACTAGTCGCGTC**

*Bold sequence indicates the Spinach sequence that is used in all sensors, and italic sequences indicate metabolite-specific sequences.

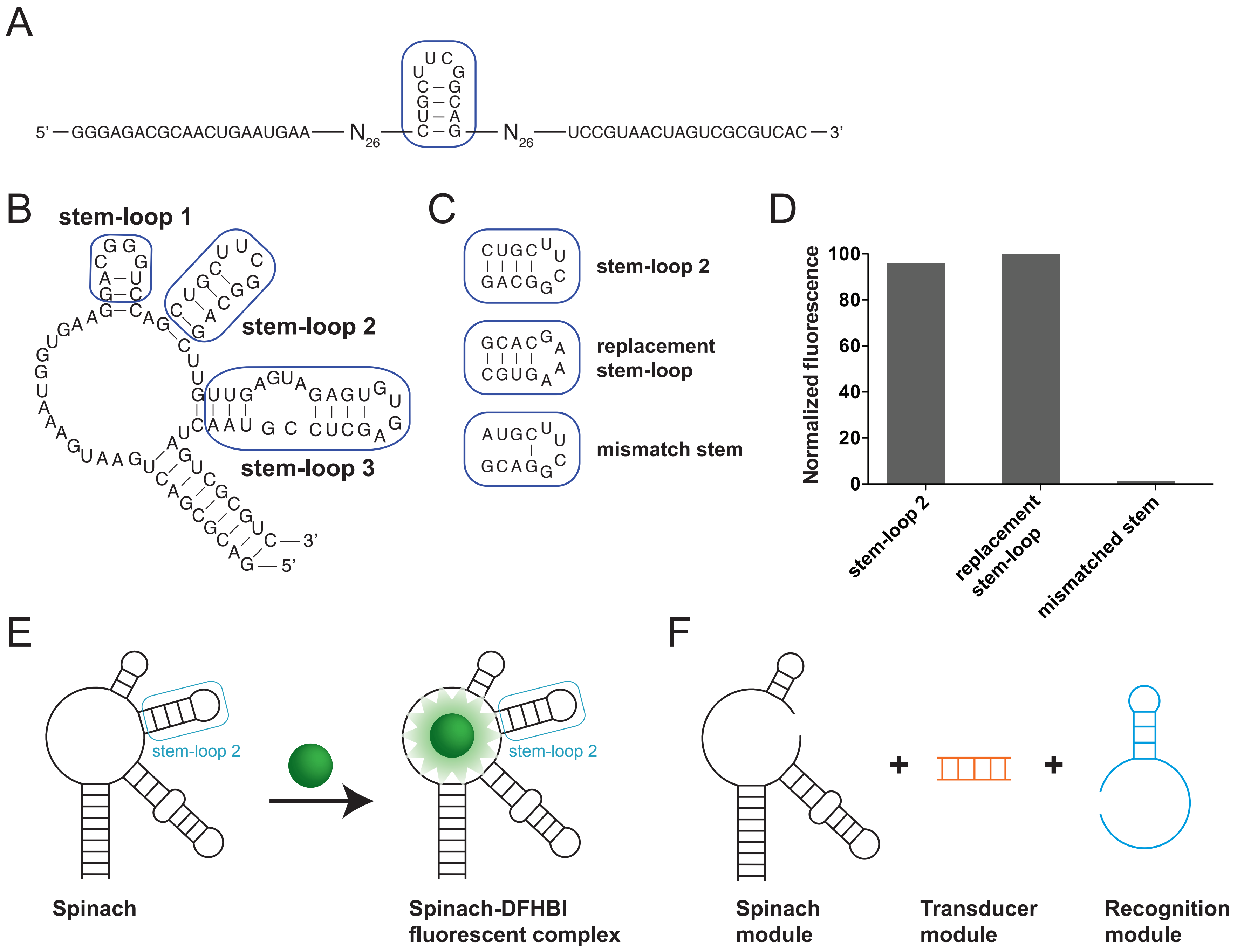

Paige, *et al*. Fig. S1

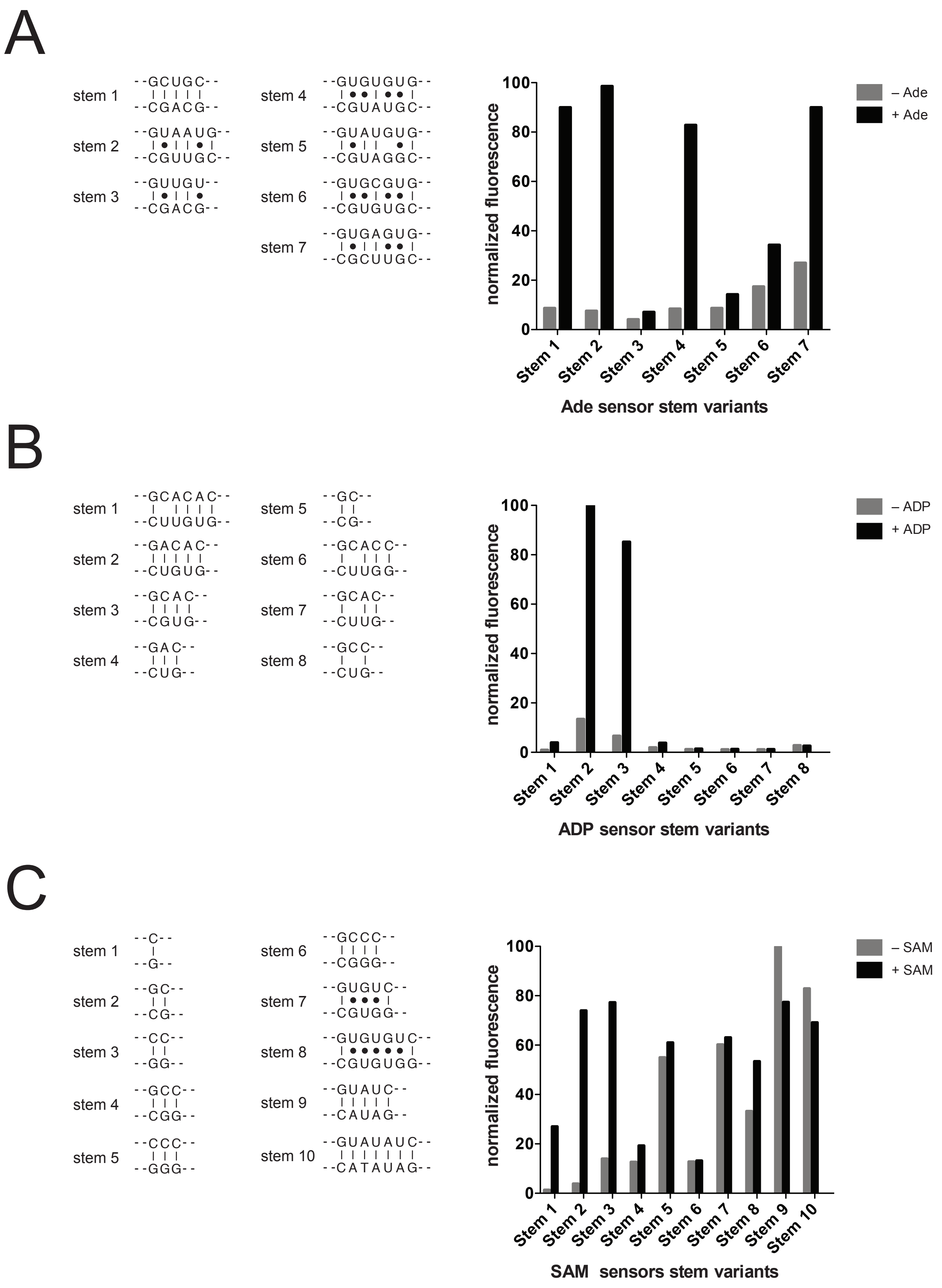

Paige, *et al*. Fig. S2

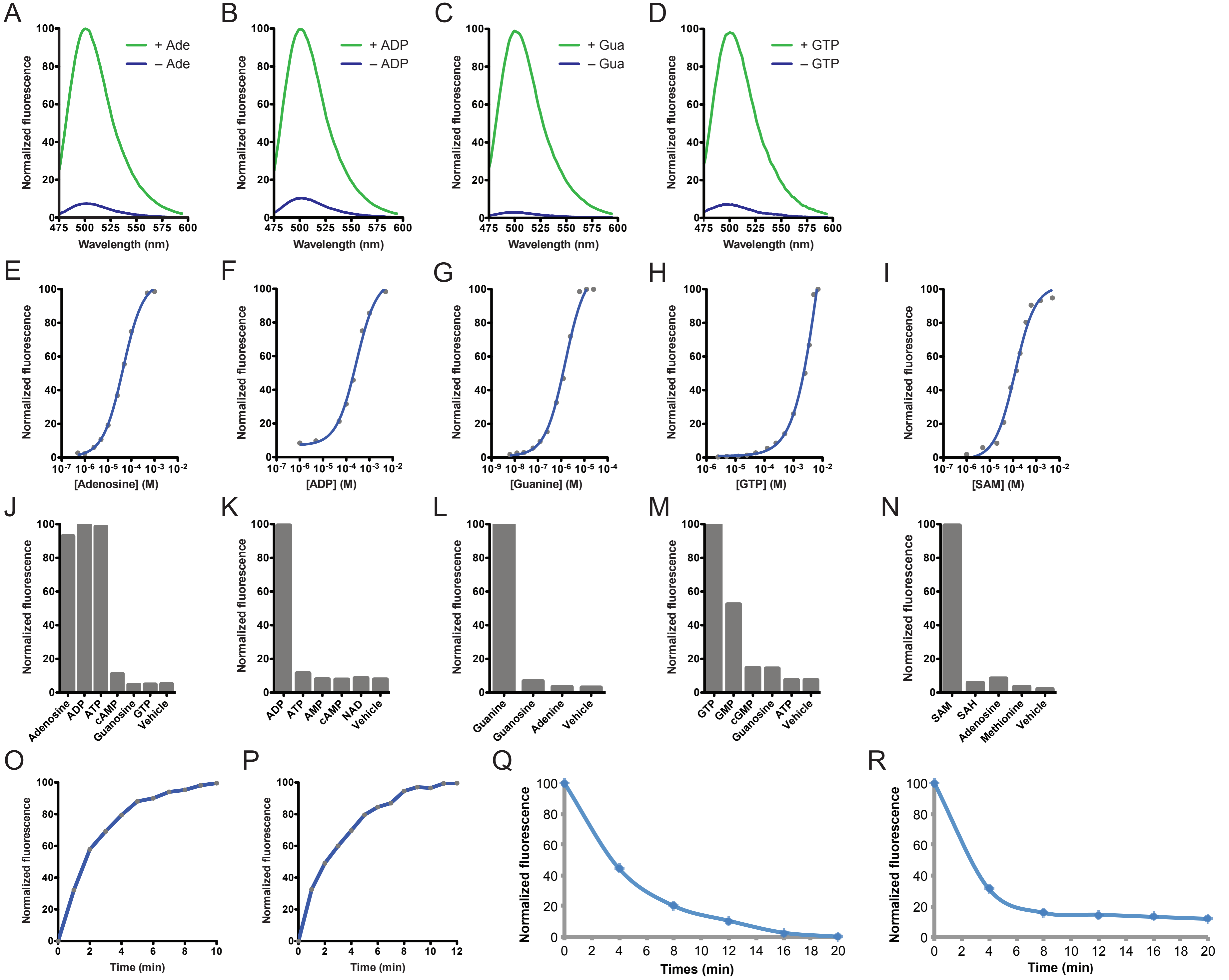

Paige, *et al*. Fig. S3

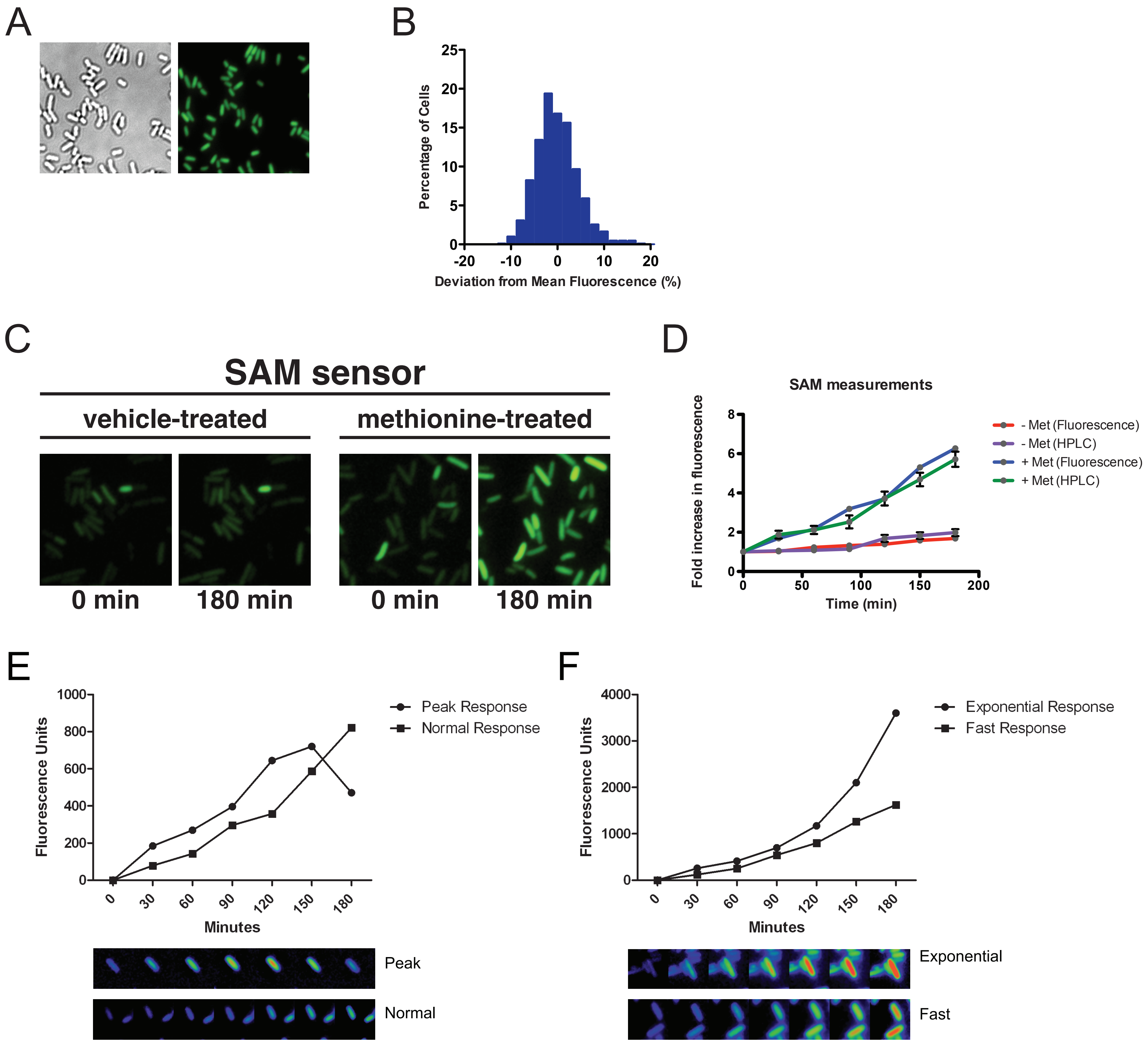

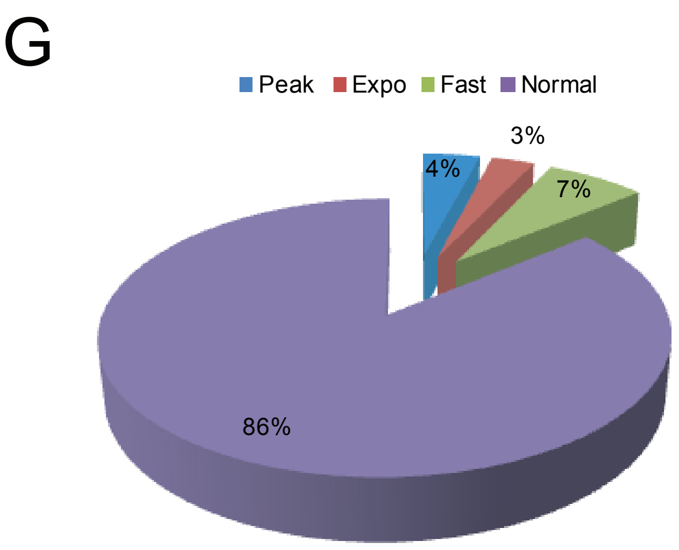

Paige, *et al*. Fig. S4

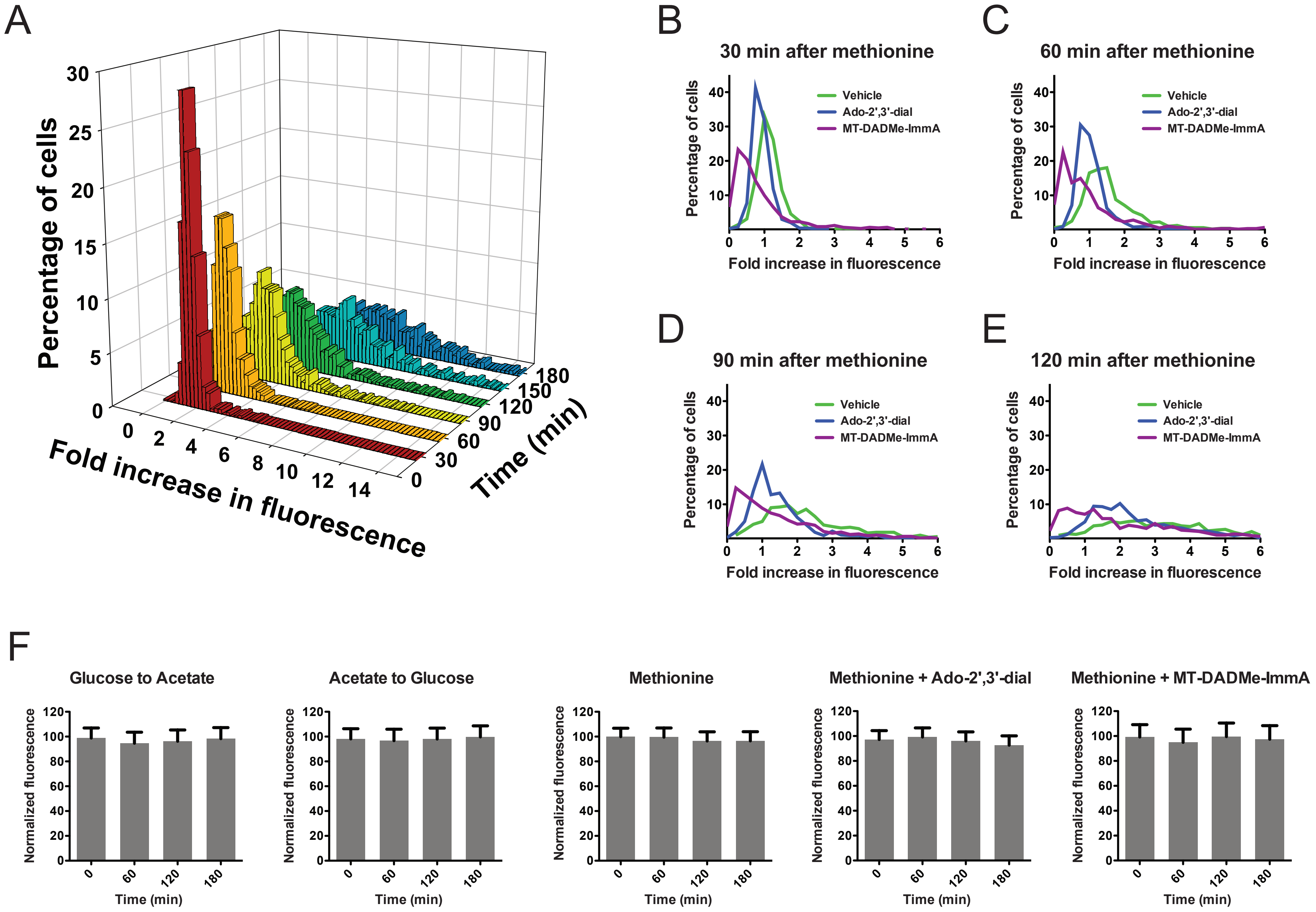

Paige, *et al*. Fig. S5

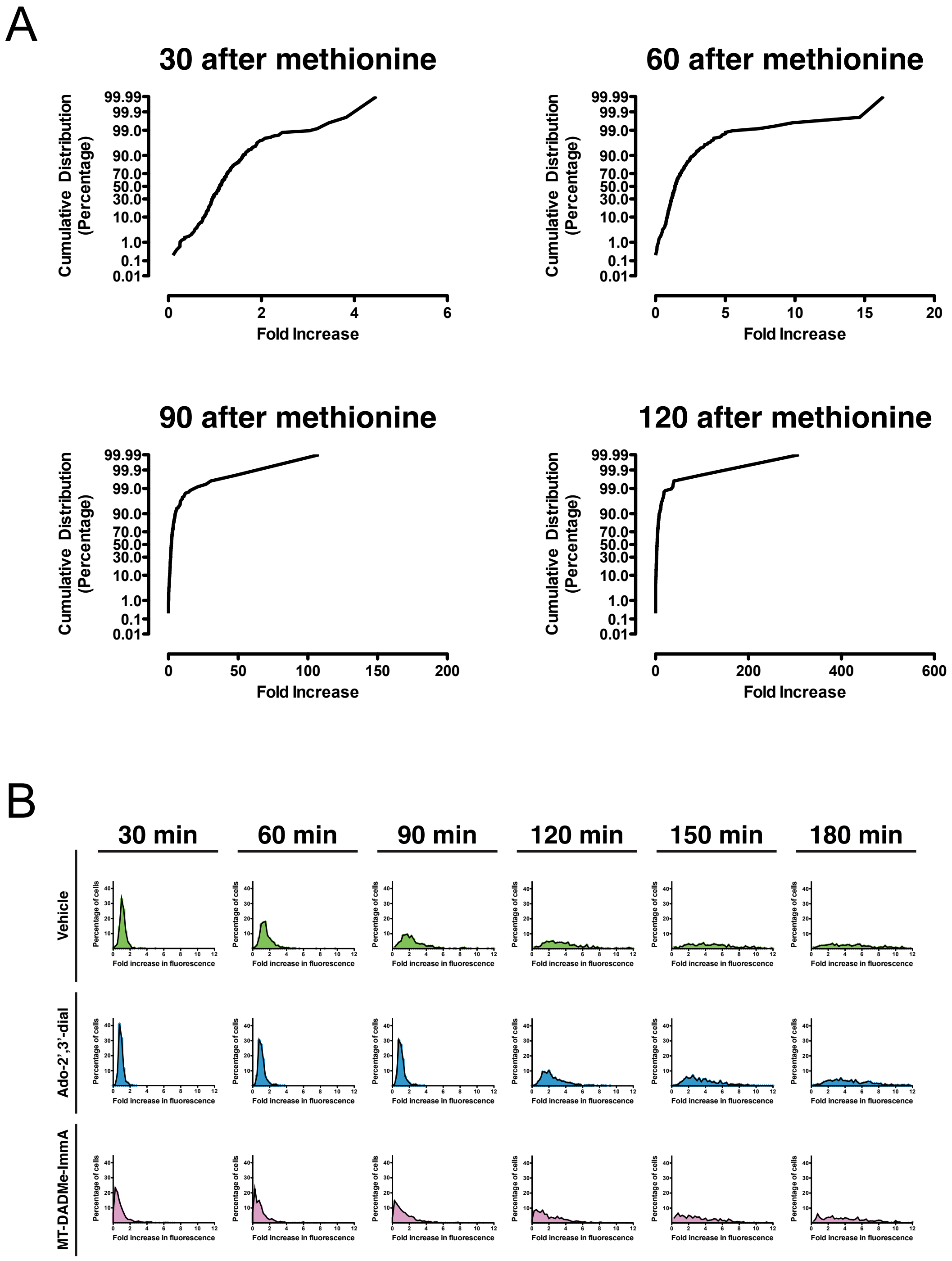

Paige, *et. al*. Fig. S6

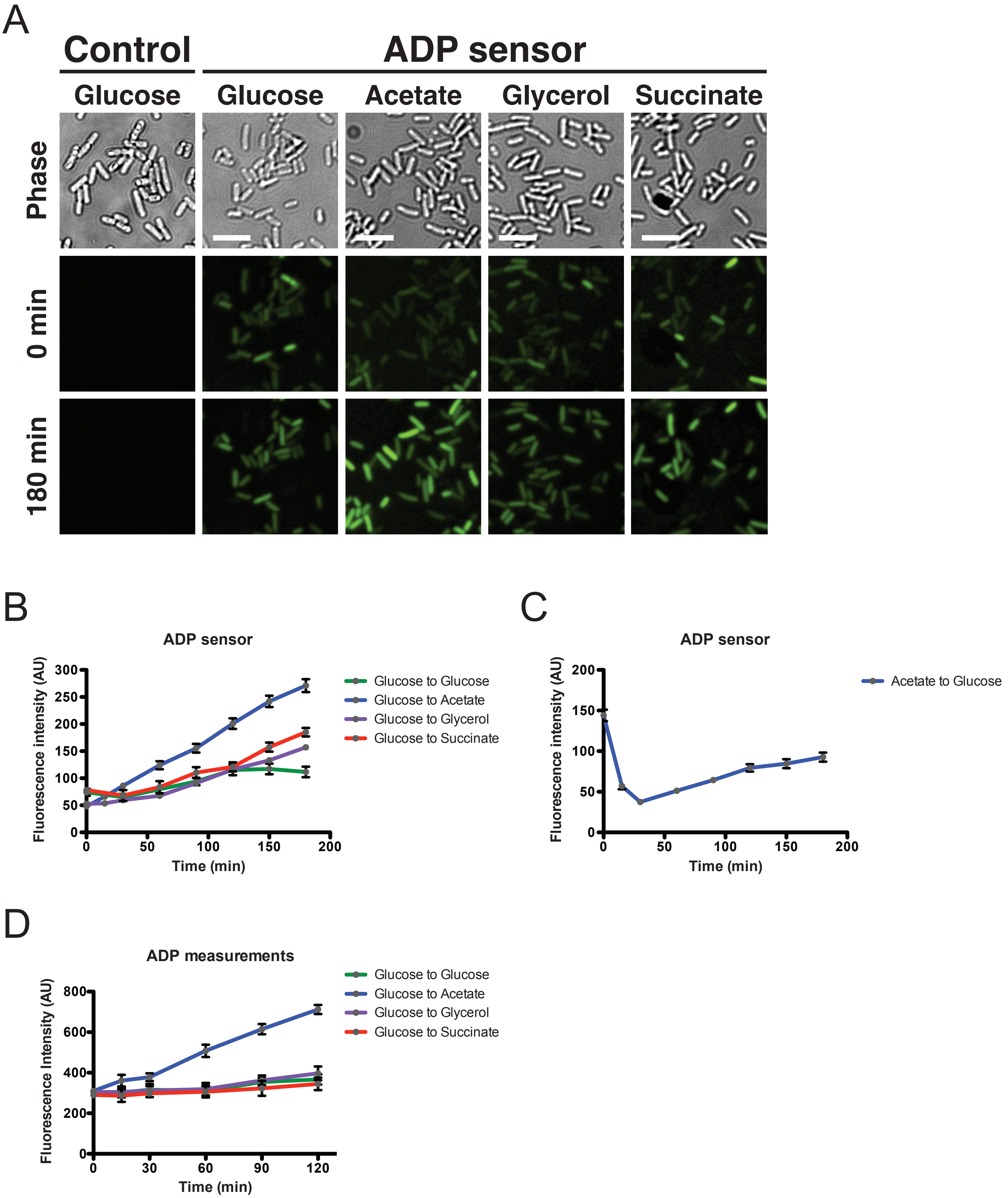

Paige, *et al*. Fig. S7